



**HAL**  
open science

## High index spin-on photosensitive material and process optimization for image sensor devices

B. Mortini, C. Aumont, J.-P. Reynard, E. Mortini, A. Crocherie, A. Hirigoen,  
Jérôme Vaillant

### ► To cite this version:

B. Mortini, C. Aumont, J.-P. Reynard, E. Mortini, A. Crocherie, et al.. High index spin-on photosensitive material and process optimization for image sensor devices. *Journal of Photopolymer Science and Technology*, 2009, 22 (6), pp.707-711. 10.2494/photopolymer.22.707 . hal-04515172

**HAL Id: hal-04515172**

**<https://hal.science/hal-04515172>**

Submitted on 21 Mar 2024

**HAL** is a multi-disciplinary open access archive for the deposit and dissemination of scientific research documents, whether they are published or not. The documents may come from teaching and research institutions in France or abroad, or from public or private research centers.

L'archive ouverte pluridisciplinaire **HAL**, est destinée au dépôt et à la diffusion de documents scientifiques de niveau recherche, publiés ou non, émanant des établissements d'enseignement et de recherche français ou étrangers, des laboratoires publics ou privés.

# High Index Spin-on Photosensitive Material and Process Optimization for Image Sensor Devices

B. Mortini<sup>1</sup>, C. Aumont<sup>1</sup>, J.-P. Reynard<sup>1</sup>, E. Mortini<sup>1</sup>, A. Crocherie<sup>1,2</sup>, F. Hirigoyen<sup>1</sup>, J. Vaillant<sup>1</sup>

<sup>1</sup> STMicroelectronics, 850 rue Jean Monnet, 38920 Crolles, France.

<sup>2</sup> CEA-LETI-DOPT 17, rue des Martyrs, 38054 Grenoble, France

This paper presents the developments of a new high refractive index material that can be used as a light guide in the back-end of CMOS image sensor to achieve optical path improvement and better light collection. Depending on the process conditions, the refractive index of the material can be tuned from 1.6 to 1.8 (RI @ 633nm). Moreover, this material can be patterned when exposed to i-line leading to a very simple and efficient cost of ownership process in the device fabrication flow. Material characteristics as well as patterning performance of a high refractive index precursor material are discussed here in the frame of a 1.4  $\mu\text{m}$  pixel technology development.

**Key words:** refractive index, image sensor devices, spin-on material, photosensitivity

## 1. Introduction

The image sensor market has been growing steadily over the last years due to the increasing demands of digital still and cameras, especially mobile cameras. At the same time, the companies addressing this market have to satisfy strong price pressure and higher resolution sensors with improved image quality and smaller size [1, 2]. Charged-Coupled Devices (CCD) have been the dominant image sensor technology, nevertheless Complementary Metal Oxide Semiconductor (CMOS) technology has reached competitive performance and show advantages such as on-chip functionality possibilities and low power consumption [3, 4]. A CMOS image sensor is composed of an array of pixels (light sensitive elements) surrounded by a read-out circuitry. Each pixel is made of a photodiode which collects the photogenerated electrons and of transistors dedicated to collect, convert and read these electrons. organic color filters are placed above the pixel for color reconstruction [5] and microlenses are placed on top to concentrate light flux to the photodiode (Figure 1). Another approach proposes to use two microlens levels, above and below the color filter area [6]. These solutions are limited by diffraction and strongly dependent on microlens shape and diameter. There are also optical losses in the stack by reflection and diffraction due to interconnect metal layers and losses by absorption due to some dielectric layers. As a result, it can be interesting to introduce a light guide to drive the light towards the photodiode. This architecture relies on the total reflection of the light between a high index material (used in the light guide) and a material with a lower refractive index (here, the dielectric stack). Previous work has reported results with a material with refractive index value of about 1.65 at 650nm [7]. In this study, our objective was to develop a process using a material with an average refractive index in the visible above 1.7. In this paper, after presenting some simulation results showing the expected gain of the light guide, we will review the characteristics of the material we selected and present the first results we obtained.

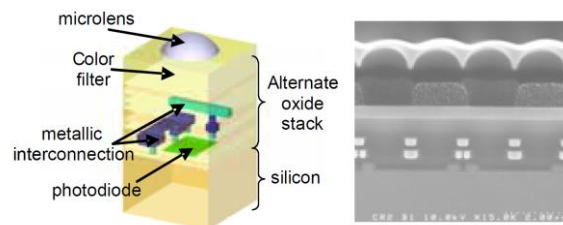


Figure 1: CMOS image sensor: schematic (left) and SEM cross-section view (right)

## 2. Experimental

### 2.1 Materials and Processes

High index precursor material (XIM4) used in this work was supplied by Pryog, LLC. XIM4 is based on zirconia and hafnia compositions that are sensitive to g-line, i-line and KrF wavelengths. The material is capable of generating high refractive index patterns after appropriate treatment (high temperature bake or plasma treatment). The detailed process is the following (Figure 2): a thin film is formed by spin coating. The post apply bake step has been set at 120°C for 120s. In our experiments, as the final film thickness should be around 1  $\mu\text{m}$  to fulfill the microcavity structures and as a large amount of the film shrinks due to pyrolysis during the final bake or plasma step, the film thickness after the post-apply bake step varies between 1.6 to 2 microns. Then the film is exposed at 365nm wavelength. The capability of the material to be developed under negative tone conditions allows avoiding an etch back step. Negative tone patterns are then developed in organic developer such as 1-methoxy-2-propanol. In these experiments, we apply a 60s static step followed by some drying steps at different spin speeds up to 1500 rpm. Then, the patterns are baked in an oven. Several temperature ramp programs were tested up to 400  $^{\circ}\text{C}$  to yield a high refractive index material. Oxygen based plasma treatments were also tested as potential replacement of the high temperature bake step.

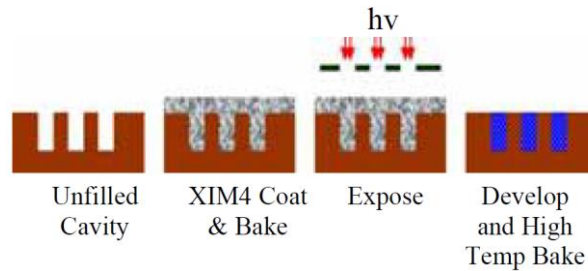


Figure 2: Steps involved in processing of the high refractive index precursor material (XIM4).

Lithographic processes were carried on TEL tracks (ACT/8 or ACT/12 depending on the wafer diameter). Two exposure tools were used depending on the wafer size: an ASML PAS5500/275 (0.48 NA) tool was used with 200mm wafers and a Nikon SF140 tool (0.43 NA) with the 300mm wafers. The oven we used was a YES tool, with nitrogen atmosphere. Considering the material characterization tools, thermogravimetry analyses were performed on a TA 2950 TGA tool. Top-down pictures and cross-sections of the samples were examined using scanning electron microscopy. A spectroscopic ellipsometer was used for RI and thickness measurement.

## 2.2 Stack description

Figure 3 shows two possible architecture options for the microcavity above the photodiode. With the first approach, a microcavity of about 2 $\mu\text{m}$  in height, 0.7 $\mu\text{m}$  in width is targeted. In the second scheme we reduce the back-end stack, decreasing the microcavity height to about 1  $\mu\text{m}$  (keeping its CD to 0.7 $\mu\text{m}$ ).

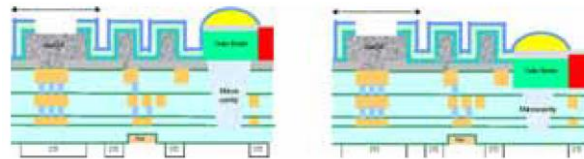


Figure 3: Architecture options. Left side: 2 microns deep microcavity through conventional back-end stack. Right side: 1  $\mu\text{m}$  deep microcavity in reduced back-end stack.

## 2.3 Simulation inputs

Optical simulations have been conducted in order to identify the most promising solutions with different back-end architectures using a Finite Difference Time Domain (FDTD) simulation model developed at STMicroelectronics. The complete methodology used for this kind of simulation has already been published [8, 9]. We perform 3D narrowband simulations at 532 $\pm$ 20nm with a diffuse-like source (i.e. incidence angle between -10 $^{\circ}$  and +10 $^{\circ}$ ) on a real pixel with color filters. The intensity distribution of the light is obtained from the Poynting vector ( $\text{W}\cdot\text{m}^{-2}$ ).

In the first case, we consider that the 2  $\mu\text{m}$  deep microcavity which acts as a lightguide is filled with a transparent material with a refractive index around 1.5. Figure 4 illustrates the Poynting results with this stack (cut in the Y direction: blue and green pixel line in a Bayer pattern and cut in the X direction: red and green pixel line). The light intensity at the silicon interface, where the photodiode is, is zero.

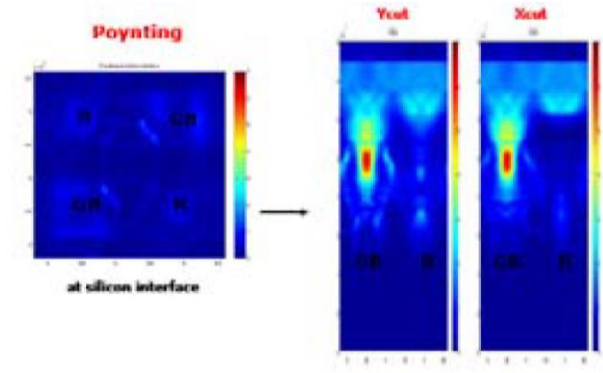


Figure 4: Poynting results from FDTD simulations with a 2  $\mu\text{m}$  deep microcavity filled with a 1.5 refractive index material.

In the second case we consider a high refractive index material ( $\sim 1.8$ ) in the 2  $\mu\text{m}$  deep microcavity. As illustrated in Figure 5, the high index material allows achieving enhanced light intensity at the silicon interface. We estimate that this effect can be interesting with materials having a refractive index of 1.7 or higher.

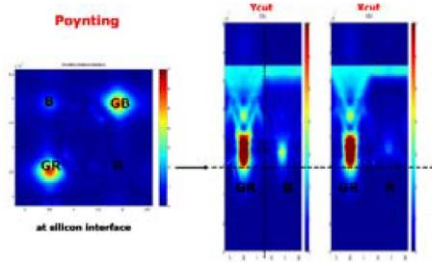


Figure 5: Poynting results from FDTD simulations with a 2  $\mu\text{m}$  deep microcavity filled with a 1.8 refractive index material.

In addition to these results, we have also demonstrated that a reduced back-end stack provides a real optical gain [10]. So the combination of the two approaches is interesting to study. As a result, there is a real interest to identify and develop a photosensitive high index material and evaluate its performances for microcavity filling and lightguide properties in a CMOS image sensor application.

### 3. Results and Discussion

#### 3.1: Filling capabilities of XIM4

Figure 6 shows the filling of 1  $\mu\text{m}$  deep microcavities after spincoating with XIM4 at 1500 rpm. On unpatterned silicon wafer, the film thickness at 1400 rpm is 2.3  $\mu\text{m}$  and the refractive index measured after post-applied bake was 1.63. Good filling properties with no voids were observed. Moreover, no differences in the film thicknesses could be observed between the edge and the center of the wafer suggesting good global planarization properties of the material.

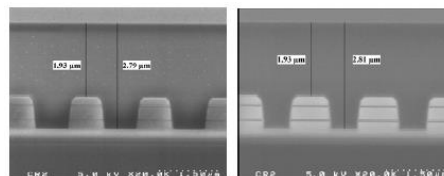


Figure 6: Cross-sections showing 1  $\mu\text{m}$  deep microcavity filled with XIM4 (spin speed: 1500 rpm, PAB: 120°C/120s).  
Left picture: wafer center. Right picture: wafer edge.

### 3.2: Lithographic Performance of XIM4

In order to develop a low cost of ownership process, it was important to identify a high index material, which was also sensitive to i-line in order to define through a single lithographic step the microcavity area. The objective was to avoid extra process steps such as etch-back, additional lithographic and etch steps. Critical dimensions in the colorization steps of the image sensor fabrication corresponded to the pixel size. As a result, the patterning capabilities of XIM4 to print 1.4 and 1.75  $\mu\text{m}$  pixel patterns were evaluated.

As illustrated in Figures 7 and 8, XIM4 successfully printed 1.75 and 1.4  $\mu\text{m}$  pixels with sharp profiles. Under these conditions, the dose to size was around  $100\text{mJ}/\text{cm}^2$ , suggesting excellent sensitivity of the material that is desirable for high throughput patterning. XIM4 also printed patterns with sufficiently large process window as confirmed by focus latitude of more than 1  $\mu\text{m}$ . From lithographic point of view, XIM4 matched our materials and process requirements.

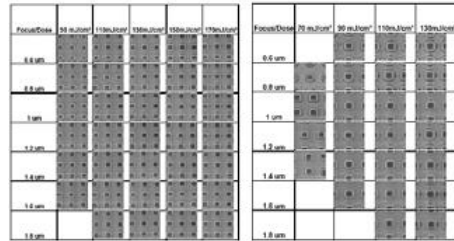


Figure 7: Topdown SEM views. FEM printed with XIM4 (spin speed: 1500 rpm, PAB:  $120^\circ\text{C}/120\text{s}$ ). Develop: 60s in PGME; Exposure Tool: ASML (0.48 NA). Left: 1.75  $\mu\text{m}$  pixels; Right: 1.40  $\mu\text{m}$  pixels.

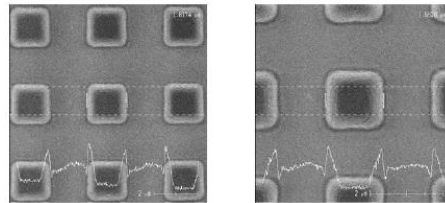


Figure 8: Topdown SEM views. 1.75 $\mu\text{m}$  (left side) and 1.4 $\mu\text{m}$  (right side) pixels printed with XIM4 (spin speed: 1500 rpm; PAB:  $120^\circ\text{C}/120\text{s}$ ); 0.48 NA; Best dose, Best focus ( $90\text{mJ}/\text{cm}^2$ , 1.4  $\mu\text{m}$ ).

### 3.3: Refractive Index Characteristics of XIM4

XIM4 film is mainly composed of organic and metal moieties. Refractive index of soft baked film was only 1.62. A conventional way to increase refractive index of the film is to reduce its organic component by pyrolysis via an appropriate thermal treatment.

A systematic approach was adopted to study the thermal decomposition characteristics of the material by thermogravimetric analysis (TGA) (Figure 9). TGA data was generated by applying a linear temperature ramp of  $10^\circ\text{C}/\text{min}$  to XIM4 film. The film was flood exposed at  $400\text{mJ}/\text{cm}^2$  to mimic the patterning process.

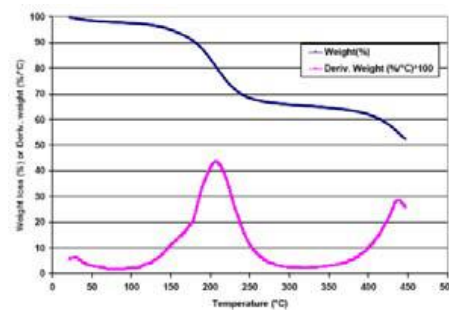


Figure 9: Thermal characteristics of XIM4 film after PAB of  $120^\circ\text{C}/120\text{s}$  and a flood exposure at  $400\text{mJ}/\text{cm}^2$  (film thickness  $\sim 2\mu\text{m}$ ).

TGA data of Figure 9 shows a strong weight loss corresponding to organic degradation at temperature range between 200 to 210°C, leading to a weight loss of about 30% of the original sample weight at 250°C. A second weight loss step is observed at a bake temperature of around 400 °C.

Preliminary thermal treatment conditions were chosen based on the TGA data. Accordingly, a linear temperature ramp of 10°C/minute up to the target temperature followed by a 20 minutes hold at the target temperature was chosen. Figure 10 shows refractive index values along with film thickness variations as a function of the bake temperature.

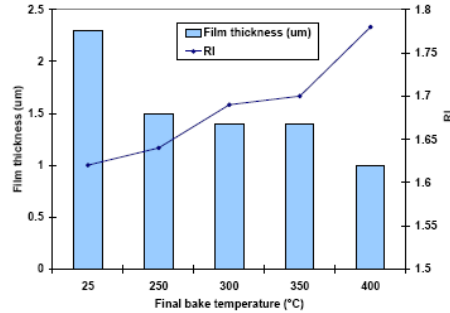


Figure 10: Variations of the refractive index at 633nm and the film thickness of XIM4 after the final bake step (linear ramp: 10°C/min + 20 minutes at target temperature).

Before applying the high temperature bake step, refractive index of the film was 1.62. After a 250°C/20min bake, there was only a marginal improvement in refractive index value to 1.64, while film thickness had dramatically shrunk from 2.3 µm to 1.5 µm.

In the next set of experiments, film was treated at 300°C and 350 °C/20min bakes. At 300°C, refractive index of the film was about 1.7. Not much improvement in refractive index was observed when film was treated at 350°C. Film thickness values at 300 and 350 °C bakes were nearly identical as it is also confirmed by lack of significant weight loss in the 300 to 350°C temperature range by TGA analysis. Interestingly, refractive index value improved significantly from 1.64 at 250 °C bake to 1.7 at 300°C bake without any additional significant film shrinkage that suggested incomplete pyrolysis of the film at 250 °C. TGA analysis suggested, the onset of the next weight loss step occurred after 350°C. Film treated at 400 °C had measured refractive index of 1.8. Under these conditions, the resist film shrinkage was about more than 50% compared to the initial film thickness. Higher refractive index value of the film at 400°C could be related to different degradation mechanism compared to those occurring at lower bake temperatures.

In parallel, replacement of the high temperature bake step to increase the refractive index of the material by an oxygen plasma treatment will be studied next. Indeed, this alternative process would have the benefit to limit the thermal budget applied to the material and thus will allow the development of new colored materials combining high refractive index values with color filter properties.

#### 4. Conclusions

Different architectures were proposed in CMOS image sensor design to maximize the light collection by the photodiode and thus increase the device performance. Among all, high index material light guide was potentially an effective solution. In this study we focused our attention on a high refractive index material based on a zirconia and hafnia compositions that also showed patterning capabilities under i-line exposures thereby simplifying our process flow. From a patterning point of view, XIM4 demonstrated good resolution capabilities and process window. XIM4 was capable of printing 1.4 µm patterns in 1.5 to 2 µm thick films. A bake step up in the temperature range of 300°C-400°C was utilized to increase the refractive index of the film in the range of 1.7-1.8. Integration of the material in the final device fabrication is under way.

#### 5. Acknowledgements

The authors would like to acknowledge the support of the management of Pryog, LLC in supplying several samples of XIM4 and for many useful discussions

## 6. References

1. A. El Gamal and H. Eltoukhy, *IEEE Circuits & Devices Magazine*, May-June, (2005)
2. E. R. Fossum, *IEEE Transactions on Electron Devices*, **44**, (1997) 1689-1698
3. E. R. Fossum, *Proc. SPIE*, **1900**, (1993)2-14
4. K. Janesick, *Optical Engineering*, **41** (06), (2002) 1203-1215
5. B. E. Bayer, *United State Patent Number 3971065*, (1976)
6. S. S. Kim, , *United State Patent Number 7358110*, (2008)
7. H. Reznik, R. S. Edelstein, M. Shach-Caplan, F. Dulberg, V. Kamenetsky, K. Karaste and J. T. Rantala, *Proc. SPIE*, **7001**, (2008)
8. F. Hirigoyen, A. Crocherie, J. Vaillant and Y. Cazaux, *Proc. SPIE-IS&T Electronic Imaging*, **6816**, (2008)
9. J. Vaillant, A. Crocherie and F. Hirigoyen, *Optics Express*, **15**, 9 (2007)
10. A. Crocherie, J. Vaillant and F. Hirigoyen, *Proc SPIE*, **7001**, (2008)